Numerical Modeling of a Radio Frequency Plasma in Argon

Robert Rhodes* and Dennis Keefer†
University of Tennessee Space Institute, Tullahoma, Tennessee

An axisymmetric, two-dimensional mathematical model of a radio frequency gas heater is described and compared with experimental data. The model includes mass, axial momentum, radial momentum, and energy conservation equations along with Maxwell's equation for the circumferential component of the electric vector potential. Buoyancy along the heater axis and radial Lorentz forces are included in the momentum equations. Ohmic heating and radiation losses are included in the energy equation. The radiation loss terms are divided into an optically thin component that leaves the gas directly and an optically thick component that is modeled as a conduction term. Results from the model agree reasonably well with data obtained from a laboratory-scale gas heater using a bluff body to stabilize the plasma. Calculated results at increased mass flow and pressure are shown to indicate the model's capability in designing larger scale heaters.

Nomenclature

a_i = imaginary part of the circumferential electric potential
a_r = real part of the circumferential electric potential
b = rms axial magnetic field
D = turbulent dissipation
f_z = radial Lorentz force
G_ϕ = transport coefficients
h_i = imaginary part of the axial magnetic field
h_r = real part of the axial magnetic field
h_t = total enthalpy
K = turbulent kinetic energy
k = laminar thermal diffusivity
k_e = equivalent thermal diffusivity
q_a = specific absorbed power
q_{at} = total absorbed power
q_r = specific radiation loss
r = radial distance
S_ϕ = source term in the fluid mechanical partial differential equations
u = axial velocity
v = radial velocity
x = axial distance
μ = permeability of space
μ_e = equivalent viscosity
μ_l = laminar viscosity
u_t = turbulent viscosity
ρ = density
σ = electrical conductivity
ϕ = any fluid mechanical variable
ω = frequency x2π

Introduction

A RENEWED interest in hypersonic airbreathing vehicles, as typified by the National Aerospace Plane (NASP), has also renewed interest in methods to heat high-pressure air for the simulation of high-Mach number flight in ground test facilities. Storage heaters for air produce relatively uncontaminated air but are limited by available materials to about 2000 K. Some improvement can be obtained by heating nitrogen and oxygen separately using carbon in the nitrogen heater. Vitiation heaters have roughly the same temperature limitations and also produce a gas with physical and chemical properties quite different from air. For total temperatures above 3000 K, the most viable approach is the direct electric heating of air either with an arc heater or potentially with an electrodeless arc (radio frequency heating). Radio frequency (rf) heating has the potential to provide a source of high-temperature gas without the electrode contamination present in conventional arc heaters.

Low-pressure electrodeless gas discharges, sustained by inductive and capacitive radio frequency fields, have been known for many decades. In 1962, Reed[1] was able to sustain an inductively coupled arc in atmospheric pressure argon using a swirl flow to stabilize the plasma. The Reed plasma torch has found extensive application as a source for use in analytic spectroscopy, where it is known as an induction coupled plasma (ICP). Vortex stabilization of the plasma proved unsatisfactory for induction coupled plasmas of larger size, power, and flow, and Keefer[2] utilized a bluff body, analogous to a combustion flameholder, to improve the stability and conducted a series of experiments to determine the efficiency of the electrodeless arc as a high-temperature gas heater. Proper operation of the heater requires that the gas be hot enough to be ionized but not so hot that an excessive amount of energy is lost through radiation. A numerical model of the process will provide a design tool to aid in optimizing a heater design.

An rf heater for gases consists of a nonconducting chamber through which the gas flows, surrounded by a coil connected to an rf power supply. The coil provides an alternating magnetic field nominally parallel to the axis of the coil which induces a circumferential current in the gas flowing along the coil axis. The magnitude and radial distribution of this current depends on the conductivity of the gas, which in turn depends on its level of ionization and, hence, on its temperature. The temperature distribution results from a balance between the ohmic heating and the heat losses from convection, conduction, and radiation. As a result, there is very strong coupling between the energy input and the electromagnetic potential. This is compounded by the desire to operate the heater at relatively low temperatures where gas conductivity varies strongly with temperature.

Presented as Paper 88-0726 at the AIAA 26th Aerospace Sciences Meeting, Reno, NV, Jan. 11–14, 1988; received Sept. 12, 1988; revision received Feb. 13, 1989.

*Senior Engineer. Member AIAA.
†Professor, Engineering Science and Mechanics. Member AIAA.

This paper describes a numerical model of a bluff body stabilized plasma in a cylindrical geometry. The model provides a solution to the Navier-Stokes and Maxwell equations. The procedure is similar to that used by Wei et al.[3] except that in this model the electric and magnetic fields vary in the axial as well as the radial direction.

Theoretical Model

To define the flowfield, the temperature distribution, and the electric and magnetic fields requires the simultaneous solution of the Navier-Stokes and Maxwell equations. The present solution is restricted to the axisymmetric, two-dimensional form of the continuity, momentum, and energy equations with the addition of the electromagnetic field equations. Only the variation of the circumferential component of the vector potential field in the axial and radial direction is considered. The flow is viscous, and plasma radiation losses are divided into an optically thin component that radiates directly to the wall and an optically thick component that is incorporated into an equivalent gas thermal conductivity. The flow may be characterized as low-speed, viscous, and mathematically elliptical in nature, which makes the SIMPLE[4] algorithm a natural choice for its solution.

Governing Equations

The turbulent Reynolds-averaged equations for mass, radial and axial momentum, energy, turbulence energy, and turbulence dissipation for two-dimensional axisymmetric flow, using the Spalding k/e turbulent viscosity model[5] and for flow without swirl, are

$$\partial(\rho u r\phi)/\partial x + \partial(\rho v r\phi)/\partial r - \partial(rG_\phi \partial\phi/\partial x)/\partial x - \partial(rG_\phi \partial\phi/\partial r)/\partial r = S_\phi \quad (1)$$

where ϕ is u, v, h_t, K, *or* D. The source terms S_ϕ and the effective turbulent transport terms G_ϕ are listed for each of the variables in Table 1.

The electromagnetic field is governed by Maxwell's equations[6] and the inductive discharge is usually described by a complex second-order differential equation for the electric field.[3] However, we find it more convenient to describe the electromagnetic fields using the vector potential,[6] where the electric field $\boldsymbol{E}$ and the magnetic induction $\boldsymbol{B}$ are related to the complex vector potential $\boldsymbol{A}$ by

$$\boldsymbol{E} = -\frac{\partial \boldsymbol{A}}{\partial t} \quad (2)$$

$$\boldsymbol{B} = \nabla \times \boldsymbol{A} \quad (3)$$

Table 1 Viscous and source terms

ϕ	G_ϕ	S_ϕ
1	0	0
u	μ_e	$-\frac{\partial p}{\partial x} + \rho g$
v	μ_e	$-\frac{\partial p}{\partial r} + f_z - 2\mu_e v/r^2$
h_t	k_e	$q_a - q_r$
K	μ_e/σ_k	$G - \rho D$
D	μ_e/σ_e	$(c_1 GD - c_2 \rho D^2)/K$

From the K/e model:

$$G = \mu_e \left[2\left\{\left(\frac{\partial u}{\partial x}\right)^2 + \left(\frac{\partial v}{\partial r}\right)^2 + \left(\frac{v}{r}\right)^2\right\} + \left(\frac{\partial u}{\partial r} + \frac{\partial v}{\partial x}\right)^2\right], \quad c_1 = 1.44,$$

$c_2 = 1.92$, $c_\mu = .09$, $\sigma_k = 1$, $\sigma_e = 1.217$.

The governing equation for the vector potential is given by[6]

$$\nabla^2 \boldsymbol{A} - \mu\epsilon \frac{\partial^2 \boldsymbol{A}}{\partial t^2} = \mu \boldsymbol{J} \quad (4)$$

where μ and ϵ are the permeability and permittivity of the medium and $\boldsymbol{J}$ is the current density.

If we assume that there is no azimuthal component of the magnetic field and neglect the axial component of the electric field (this is often accomplished in practice through the use of a Faraday shield), then the only nonvanishing component of the vector potential is the azimuthal component, which can be written as

$$A_\phi = [a_r(r,z) + ia_i(r,z)]e^{i\omega t} \quad (5)$$

where the spatially dependent part has been divided into a real component a_r and an imaginary part a_i and ω is the radian frequency. Use of Eq. (5) in Eq. (4) yields a pair of coupled equations for the real and imaginary components of the vector potential:

$$r^2\partial^2 a_r/\partial r^2 + r\partial a_r/\partial r + r^2\partial^2 a_r/\partial x^2 - a_r + (r^2/s^2)a_i = 0 \quad (6)$$

and

$$r^2\partial^2 a_i/\partial r^2 + r\partial a_i/\partial r + r^2\partial^2 a_i/\partial x^2 - a_i + (r^2/s^2)a_r = 0 \quad (7)$$

where

$$s^2 = 1/(\omega\sigma\mu)$$

Boundary Conditions

The following boundary conditions are applied for the geometry shown in Fig. 1. The normal pressure gradient is set to zero at all bounding surfaces. A value of pressure is set at a single point, usually on the inlet plane. Velocities tangential to a wall are given a value of zero on the wall. Velocities normal to a wall are given a zero-normal gradient. Both axial and radial velocity are specified at the inlet, the radial velocity gradient is set to zero at the outlet, and the outlet axial velocity is adjusted to conserve the total mass flow through the vessel. The wall total enthalpy is given a value equal to the gas total enthalpy at the wall temperature for cases where wall temperature is specified, and the heat flux may be set to zero at the wall when an adiabatic wall condition is desired. All of the gasdynamic variables have a zero-normal gradient at the center of axial symmetry. These conditions, as well as those for turbulent kinetic energy and dissipation, follow those used in the combustor configuration of Lilley and Rhode.[7] The

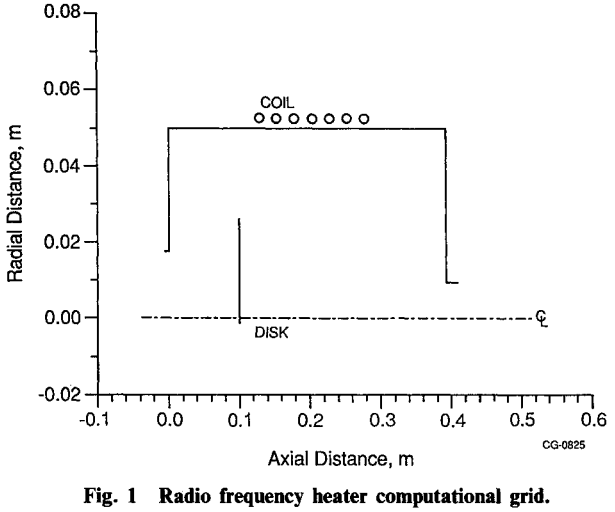

Fig. 1 Radio frequency heater computational grid.

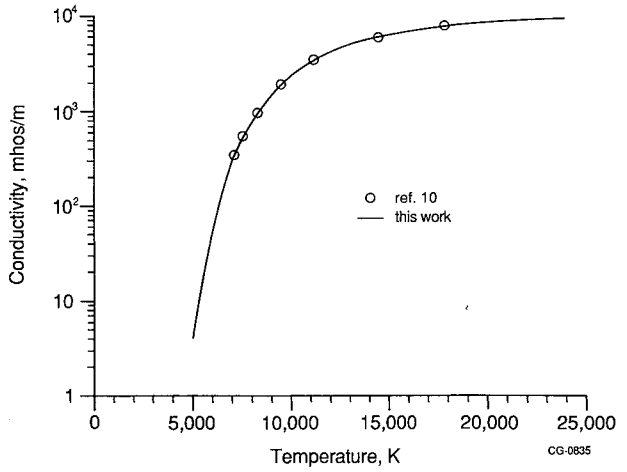

Fig. 2 Argon conductivity: 1 atm.

phase of the electric potential is arbitrary, so a value is selected for a_i on that part of the wall surrounded by the Faraday cage and is zero at all other points on the boundary. This implies a constant circulating current in the Faraday cage, which should be achievable with the proper configuration. The problem of coupling the power supply to obtain this current is not addressed in this work. The value of a_r is set to zero at all points on the boundary. Both a_i and a_r are zero on the centerline. The disk is treated as a wall with two surfaces normal to the axis of the chamber and zero thickness, so that the velocity and pressure boundary treatment is the same as on the end walls of the chamber. The disk is assumed to be actively cooled and has an isothermal boundary condition similar to the end walls of the tube. It is assumed that the disk has no effect on the electric potential so that computational regions in contact with the disk are treated the same as any other region not on a boundary.

Ancillary Relations

The thermodynamic and transport properties of the 1-atm argon used in this work are those used in Jeng's study of the laser-heated plasma.[8] The gas density ρ, laminar viscosity μ_l, thermal diffusivity k, electrical conductivity σ, and radiated power q_r are tabulated at 100 K temperature intervals and interpolated from these tables at the grid point temperature when they are required by the computation.

The thermodynamic properties (enthalpy and density) were obtained from Drellishak et al.[9] and viscosity and electrical conductivity from De Voto.[10] The electrical conductivity data were fitted to the empirical equation

$$\sigma = \exp[9.103 + (12{,}289 - 2.546 \times 10^8/T)/T)] \quad (8)$$

The consequences of the extreme sensitivity of conductivity to temperature (Fig. 2) will be discussed in the section on solution procedure.

The detailed radiative transport of energy from the plasma to the walls of the confinement vessel is beyond the capability of this computational procedure so that a simplifying assumption was made to account for this loss mechanism. The radiation from the plasma is assumed to be divided into an optically thick and an optically thin component. The optically thin part, which is principally in the visible and infrared part of the spectrum, represents direct radiation to the walls where the energy lost from a volume of gas is a function of the temperature and pressure of the gas. The ultraviolet radiation is assumed to be optically thick and is modeled as a temperature- and pressure-dependent term that augments the thermal conductivity so that the energy transport to or from a volume of gas depends on the temperature gradient as well as the local state of gas. For argon above 5000 K, the radiative component of the effective thermal conductivity becomes the dominant part of this transport coefficient. The derivation of an equivalent thermal conductivity from radiative transport in the optically thick limit is described by Özişik.[11] The optically thin radiation loss q_r was obtained from Kozlov et al.[12] and the effective thermal conductivity from Bues et al.[13]

The source terms for the differential equations are obtained using the following expressions. When the turbulent flow option is being used, the turbulent viscosity (μ_t) is

$$\mu_t = c_\mu \rho K^2/D \quad (9)$$

$$\mu_e = \mu_l + \mu_t \quad (10)$$

$$k_e = k + \mu_t \quad (11)$$

The electrical power absorbed per unit volume of gas is

$$q_a = 0.5\omega^2\sigma(a_i^2 + a_r^2) \quad (12)$$

and the total power absorbed is

$$q_{at} = \int\int_{\text{volume}} q_a \partial x \partial r \quad (13)$$

The real and imaginary parts of the axial magnetic field vector are

$$h_r = r\partial(ra_r)/\partial r \quad (14)$$

and

$$h_i = r\partial(ra_i)/\partial r \quad (15)$$

The rms magnetic field is

$$b = \sqrt{(h_r^2 + h_i^2)} \quad (16)$$

The Lorentz force on the gas in the radical direction is

$$f_z = 0.5\sigma\omega(h_r a_i - h_i a_r) \quad (17)$$

Solution Procedure

The set of partial differential equations is solved using the SIMPLE algorithm derived from the work of Jeng and Keefer[8] and Lilley and Rhode.[7] The electromagnetic equations used to calculate a_r and a_i were incorporated into the program and solved in a manner similar to the equations containing the fluid mechanical variables.

Because of the strong coupling between the electromagnetic equations and the energy equation, it was not possible, with the unmodified equations, to obtain solutions for cases where the peak temperature was less than about 10,000 K. The change in conductivity with temperature is very large at the lower temperatures. The coupling between temperature, conductivity, and absorbed power results in positive feedback to perturbations which makes stable solutions nearly impossible to achieve in this temperature range. Since the cases of interest are believed to have peak temperatures between 7500 and 8500 K, it was necessary to partly decouple the equations during the iteration procedure. This was accomplished by defining the power level desired and assuming an initial boundary value for a_i ($a_{i\,\text{wall}}$). The integral of the absorbed power resulting from the a and σ fields is calculated at each iteration step, and the power absorbed at each grid point is multiplied by the ratio of the desired power to this calculated integral power. This produces a solution that is incorrect, in that there is a multiplier in Eq. (8) that does not belong there. This solution is modified by changing $a_{i\,\text{wall}}$ until the ratio of the integral absorbed power to the desired power, and hence the multiplier, becomes 1.

Calculated Results and Comparison with Experiment

The ultimate purpose of the rf heater model is to provide an analytical description of the flowfield and temperature distribution in a proposed heater design. The calculated results can be used to evaluate the effect of scaling of size, mass flow, and pressure on power requirements and thermal efficiency. The differences in operation with different gases can be investigated as well as the effects of the geometry of the containment vessel and the rf coil and the power supply frequency. In order to have any confidence in the results of these calculations, the model must be verified. Unfortunately, there is no detailed data on the velocity or temperature fields in an rf gas heater, and the evaluation must be done using a less rigorous procedure.

Description of the Experiment

In the early 1970's the second author (Keefer, then at the University of Florida) performed experiments on rf gas heating, sponsored by Arnold Engineering Development Center (AEDC).[2,14] The data consists of gas flow rate, final gas bulk temperature calculated from the known flow rate and pressure-feeding a choked orifice at the discharge of the heater, and visual and photographic observations of the heater in operation. The rf power absorbed by the driving coil was also measured. The heater consisted of a Pyrex cylinder with an axisymmetric baffle designed to produce a recirculation zone in the center of the tube just upstream of the region of heat input. The idea behind this is based on the similarity between the rf heating process and a combustion zone, where the rate at which the gases are heated by the electric current and the rate at which they release heat by combustion both increase strongly with temperature and the recirculation of heated gases provides the preheating necessary for stabilization. Argon was metered into the tube through an annulus around a tube which supported and provided cooling water for the baffle. The viability of the idea of "flame holding" was verified by the observation that with the baffle the heater was completely stable and could not be blown out with the available gas supply, and would only go out when the input power was reduced. Without the baffle, it was nearly impossible to maintain a stable heating zone in the tube.

Comparison with Calculations

The rf heater model was used to calculate the flow and thermal field in this configuration for one of the higher-power cases for which there is data. The geometry is modeled as closely as possible (Fig. 1). The model calculation does not have the axisymmetric tube supporting the baffle and has a discharge orifice that is not choked. It is not possible to specify pressure, mass flow, and the size of a choked orifice simultaneously, and it was decided to use pressure and mass flow, which are both known from the experiment. Also, with the computational grid of the SIMPLE algorithm, it is very difficult to adequately cover the large range of scales involved in a very high area ratio contraction. The calculation was made for argon with a total mass flow of 0.6 g/s, a pressure of 1 atm, and an rf power input of 6.28 kW. All of the calculations were made assuming laminar transport properties. This was done since these cases have relatively low flow rates where the flow might be expected to be laminar, and the extra equations add considerably to the computational time and ease of convergence.

These calculations were made on a Cray XMP/12 computer system. The gridding used has 81 steps in the axial direction and 61 in the radial direction. The radial grid spacing is reduced by 5% per step from the centerline outward to provide a fine grid near the outer boundary. There are 20 evenly spaced grid points upstream of the disk and 61 grid points between the disk and the exit plane which increase in size toward the exit at 1% per step. The calculations for this case required about 3 min for 1000 iterations, and 20,000 iterations were required to obtain a resonable level of convergence.

The temperature field and velocity vectors from the calculation are shown in Fig. 3. The 7000 K isotherm very closely matches the shape and size of the observed plasma (Fig. 4). The peak temperature is away from center of the tube and near the center of the rf coil. The velocity vectors clearly show the strong recirculation zone behind the disk and a weak recirculation zone along the downstream wall of the tube. The Lorentz forces on the plasma apparently deflect the flow inward at the regions of high temperature where the circulating currents are highest and help deflect the cool flow along the wall into the heating zone.

The experimental bulk temperature from the experiment was 4233 K, which compares with the calculated value of

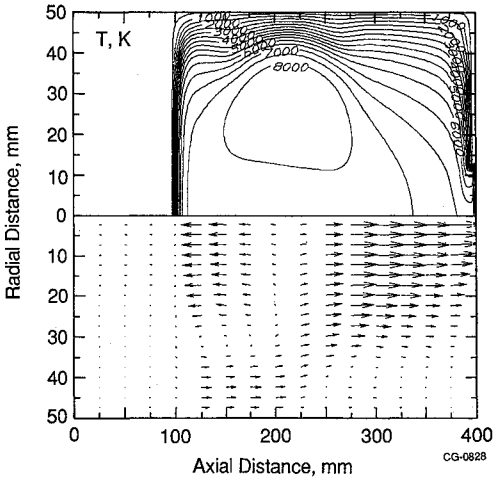

Fig. 3 Temperature contours and velocity vectors: 61 × 81 grid, 1 atm, 0.6 g/s, 6.28 kW.

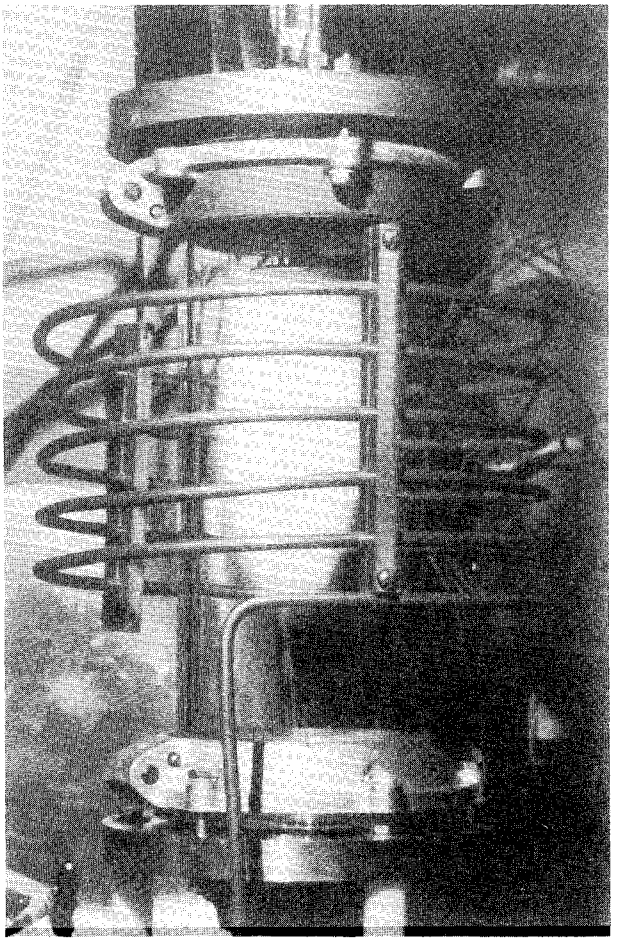

Fig. 4 Typical bluff-body-stabilized discharge.

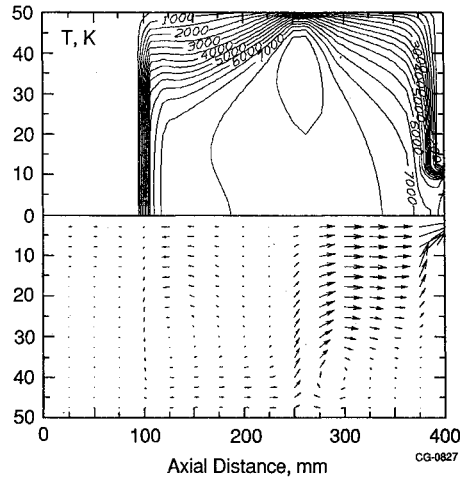

Fig. 5 Temperature contours and velocity vectors: 31 × 21 grid, 1 atm, 0.6 g/s, 6.28 kW.

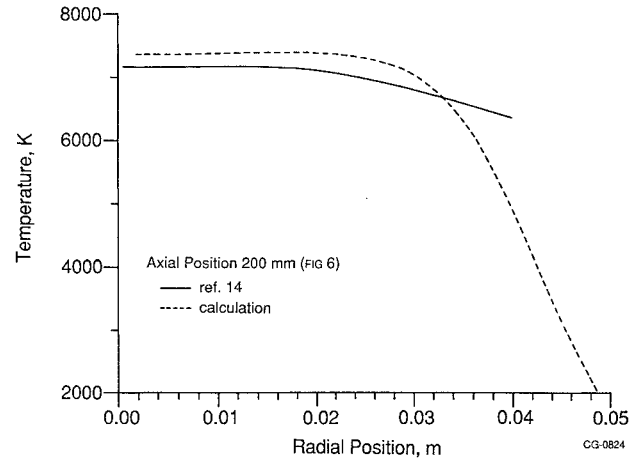

Fig. 7 Radial temperature profile: 1 atm, 0.2 g/s, 2.1 kW.

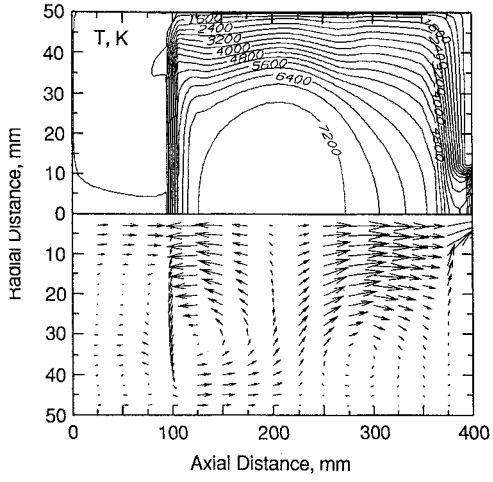

Fig. 6 Temperature contours and velocity vectors: 21 × 31 grid, 1 atm, 0.2 g/s, 2.1 kW.

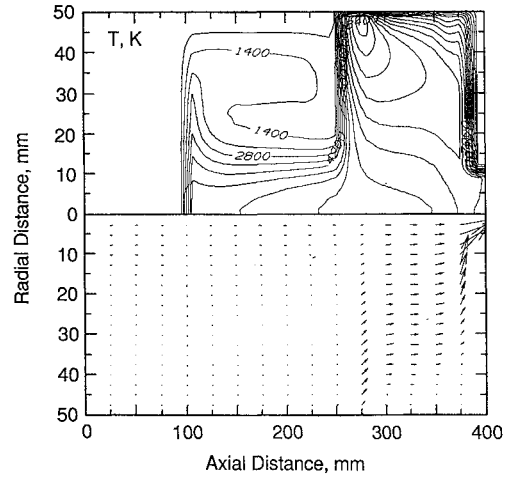

Fig. 8 Temperature contours and velocity vectors: 21 × 31 grid, 1 atm, 12 g/s, 120 kW.

5700 K. The calculation indicates that of the slightly over 6-kW input, 48% is lost by conduction to the walls and 24% lost by radiation. This gives an efficiency of 28% for the calculation compared to 21.4% for the experimental measurement. The discrepancy between the calculation and the experiment represents less than 10% of the power losses from the system. Considering the assumptions used in both the radiations and the conduction model, this agreement is quite good.

The same case was run on the University of Tennessee Space Institute MassComp computer with a 31 × 21 uniform grid. These results (Fig. 5) give a very similar temperature field, although the maximum is somewhat further downstream and nearer the wall. The calculation predicts an efficiency of 26%, which is very close to the results with the finer grid.

A second test case for which experimental data is available was run with a 21 × 31 grid. The mass flow was about 0.2 g/s and the power input 2 kW at 1-atm pressure. Temperature contours and velocity vectors (Fig. 6) indicate a well-stabilized plasma behind the disk. The inward-directed velocities in the center of the high-temperature zone clearly show the effect of the Lorentz force reinforcing the recirculation behind the disk. A radial electron temperature profile was measured for these test conditions, and the comparison between the measured and calculated temperatures (Fig. 7) is very good.

Calculated Effect of Pressure and Flow Rate

Since the ultimate objective is to provide design calculations for high-power and high-mass flow heaters, additional calculations were made on the MassComp computer with a 31 × 21 uniform grid using the same geometry as the previous cases. The first calculation was made with a pressure of 1 atm, 12-g/s mass flow and 120-kW power input (Fig. 8). The heat addition zone is located at the downstream end of the coil very near the wall and appears to be almost completely uncoupled from the recirculation zone behind the disk. There is a secondary recirculation zone near the wall apparently caused by the blockage of the heat addition zone. The relatively high velocities resulting from the increased mass flow appear to be trying to blowout the plasma. This configuration would appear to be marginally stable at best. The radiation losses are predicted to be 43% of the input power and the convection losses 17%, leaving 40% of the input power going into the gas.

More stable operation is indicated as the pressure is raised to 4 atm and the flow rate reduced to 9 g/s with the 120-kW power input (Fig. 9). There is close coupling between the disk-induced recirculation zone and the heat addition zone so that esentially all the flow is deflected radially inward by the Lorentz forces. The combination of higher pressure and a

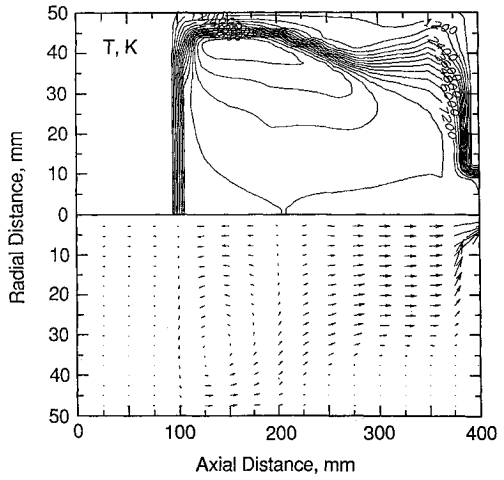

Fig. 9 Temperature contours and velocity vectors: 21 × 31 grid, 4 atm, 9 g/s, 120 kW.

larger high-temperature area increased the radiation losses to 70% of the input power. The convection losses are less than 2%, giving overall efficiency of about 28%.

Conclusions

A mathematical model of a radio frequency gas heater has been developed and the calculated results compared to the data from a laboratory-scale heater. The model was developed for two-dimensional, cylindrical coordinates and includes equations for axial and radial momentum, energy, mass continuity, and the circumferential component of the electric potential. The heater model also has the capability of solving problems where turbulence effects are important using a two-equation turbulence model.

The predictions of the model compare favorably with the experimental results from a laboratory heater using rf power to supply the energy to argon. The model results demonstrate the combined effect of a disk mounted in the flow and the Lorentz forces induced on the plasma to drive a recirculation zone that stabilizes the heat addition zone.

Since there appears to be some grid dependence in these results, some further discussion is required. The long-term stability of any interactive solution to a nonlinear set of equations is always a concern. As a result, calculations with both grids were run over 10,000 iterations. A truly stable solution was not seen in either case in the sense that the residuals reached a minimum value and oscillated about this value with additional iterations. The dependent variables also oscillated somewhat. However, the final solution was, within these limits, independent of the initial guess of the solution. There are several other factors that influence the reliability of the results of these calculations. First, compared to other conditions calculated, the two made at the same conditions with different grids are very similar. The presentation of the data as contour plots tends to magnify the differences, particularly in regions where the gradients are low. Second, the uncertainties in the radiation model and the transport properties used in the calculation put a limit on the ultimate accuracy of the results. Third, the finer grid provides a higher resolution near the walls where the gradients are high and could very well be given a more accurate solution. The purpose of this study was to develop a calculation procedure to give guidance to an experimental study of rf gas heaters by providing a cost-effective screening method for various configurations before building hardware. For this purpose, we feel but cannot prove that the method will be adequate.

The model was developed to aid in the design of gas heaters using rf electrical power for heating. The ultimate application of these heaters requires scaling over many orders of magnitude in flow and power over those developed to date. It is expected that the model, together with an experimental program, can be used to guide the design of flow and power supply configuratons to reach the required levels of input power and flow.

References

[1]Reed, T. B., "The Induction Coupled Plasma Torch," *Journal of Applied Physics*, Vol. 32, 1961, pp. 821–824.

[2]Keefer, D. R., "A Study of Electrodeless Arc Discharges Using Argon, Nitrogen and Air," Arnold Engineering Development Center, Tullahoma, TN, AEDC-TR-73-143, Sept. 1973.

[3]Wei, D., Apelian, D., and Farouk, B., "Effects of Coil Location and Injecton Flow Rate in an Inductively Coupled Plasma Torch," AIAA Paper 85-1634, July 1985.

[4]Gosman, A. D. and Pun, W. M., "Calculation of Recirculating Flows," Dept. of Mech. Eng., Imperial College, London, England, Rept. HTS/74/12, 1974.

[5]Launder, B. E., Morse, A., Rodi, W., and Spalding, D. B., "Prediction of Free Turbulent Mixing Using a Turbulent Kinetic Energy Method," *Free Turbulent Shear Flows—Vol. I Conference Proceedings*, NASA Langley Research Center, Hampton, VA, NASA SP321, 1973.

[6]Pugh, E. M. and Pugh, E. W., *Principles of Electricity and Magnetism*, Addison-Wesley, Reading, MA, 1960.

[7]Lilley, D. G. and Rhode, D. L., "A Computer Code for Swirling Turbulent Axisymmetric Flows in Practical Isothermal Combustor Geometries," NASA CR-3442, Feb. 1972.

[8]Jeng, S.-M. and Keefer, D., "Theoretical Investigation of Laser-Sustained Argon Plasmas," *Journal of Applied Physics*, Vol. 60, No. 7. 1986, pp. 2272–2279.

[9]Drellishak, K. S., Aeschliman, D. P., and Cambel, A. B., "Tables of Thermodynamic Properties of Argon, Nitrogen, and Oxygen Plasmas," Arnold Engineering Development Center, Tullahoma, TN, AEDA-TR-64-12, 1964.

[10]DeVoto, R. S., "The Transport Properties of a Partially Ionized Monatomic Gas," Ph.D. Thesis, Standord Univ., Stanford, CA, 1965.

[11]Özişik, M. N., *Radiactive Transfer and Interactions with Conduction and Convection*, Wiley, New York, 1973, pp. 316–319.

[12]Kozlov, G. I., Kuznetsov, V. A., and Masyukov, V. A., "Radiative Losses by Argon Plasma in the Emissive Model of a Continuous Optical Discharge," *Soviet Physics-JETP*, Vol. 39, 1974, pp. 417–432.

[13]Bues, J., Patt, H. J., and Richter, J., "Uber die Elektriche Leitfahigkeit und die Warmeleitfahigkeit des Argon bie Hohen Temperaturen," *Zeitschrift für Angewandte Physik*, Vol. 22, 1967, p. 345.

[14]Keefer, D. R., "An Experimental Study of Electrodeless Arc Discharges," Arnold Engineering Development Center, Tullahoma, TN, AEDC-TR-71-10, Sept. 1971.